Functional Studies of an Evolutionarily Conserved, Cytochrome b5 Domain Protein Reveal a Specific Role in Axonemal Organisation and the General Phenomenon of Post-division Axonemal Growth in Trypanosomes

Helen Farr and Keith Gull*

Sir William Dunn School of Pathology, University of Oxford, Oxford OX1 3RE, United Kingdom

Eukaryotic cilia and flagella are highly conserved structures composed of a canonical 9+2 microtubule axoneme. Several recent proteomic studies of cilia and flagella have been published, including a proteome of the flagellum of the protozoan parasite *Trypanosoma brucei*. Comparing proteomes reveals many novel proteins that appear to be widely conserved in evolution. Amongst these, we found a previously uncharacterised protein which localised to the axoneme in *T. brucei*, and therefore named it Trypanosome Axonemal protein (TAX)-2. Ablation of the protein using RNA interference in the procyclic form of the parasite has no effect on growth but causes a reduction in motility. Using transmission electron microscopy, various structural defects were seen in some axonemes, most frequently with microtubule doublets missing from the 9+2 arrangement. RNAi knockdown of TAX-2 expression in the bloodstream form of the parasite caused defects in growth and cytokinesis, a further example of the effects caused by loss of flagellar function in bloodstream form *T. brucei*. In procyclic cells we used a new set of vectors to ablate protein expression in cells expressing a GFP:TAX-2 fusion protein, which enabled us to easily quantify protein reduction and visualise axonemes made before and after RNAi induction. This establishes a useful generic technique but also revealed a specific observation that the new flagellum on the daughter trypanosome continues growth after cytokinesis. Our results provide evidence for TAX-2 function within the axoneme, where we suggest that it is involved in processes linking the outer doublet microtubules and the central pair. Cell Motil. Cytoskeleton 66: 24–35, 2009.   © 2008 Wiley-Liss, Inc.

Key words: flagellum; trypanosome; central pair; RNAi

INTRODUCTION

The axoneme which forms the core of all eukaryotic cilia and flagella is widely conserved, with the basic structure consisting of nine outer doublet microtubules with two single microtubules forming the central pair and additional structures such as inner and outer dynein arms. The growing number of genetic diseases linked to dysfunctional cilia and basal bodies has increased interest in this area [Badano et al., 2006], and recent proteomic studies in model organisms have helped shed light

on the molecular components of these enigmatic organelles.

The protozoan parasite *Trypanosoma brucei* is a useful model organism for the study of eukaryotic flagella, with many examples of the characterisation of individual flagellar proteins [Bastin et al., 1998; Hutchings et al., 2002; McKean et al., 2003; Dawe et al., 2005; Baron et al., 2007a]. *T. brucei* possesses a single flagellum which is maintained throughout the cell cycle, with a new flagellum made alongside the old flagellum prior to cell division. The publication of a *T. brucei* flagellar proteome (TbFP) containing 331 proteins [Broadhead et al., 2006], many of which are previously uncharacterised, provides a valuable resource of potentially interesting flagellar proteins. Among this list we were interested by a previously uncharacterised protein widely and exclusively conserved in flagellate organisms, which we chose for further analysis and named Trypanosome Axonemal protein (TAX)-2.

In addition to its identification from our TbFP, the *Chlamydomonas reinhardtii* TAX-2 homologue (model id: 119090) is also present in the proteome of isolated *C. reinhardtii* flagella as FAP198 [Pazour et al., 2005], and has been shown to be upregulated following deflagellation of this alga [Pazour et al., 2005; Stolc et al., 2005]. The CrFP analysis of peptides derived from differently extracted preparations revealed that TAX-2 remains with the axoneme fraction after KCl extraction [Pazour et al., 2005].

In the present study, we have validated the presence of TAX-2 in the axoneme by expression of a GFP:TAX-2 fusion protein. We then ablated protein expression of both the GFP-tagged and normal TAX-2 protein in this GFP-tagged cell line allowing a direct and easy assessment of the effect of protein ablation on cells. Such RNAi knockdown experiments reveal TAX-2 to be essential for proliferation in bloodstream but not procyclic trypanosomes. The latter form of trypanosome showed a particular slightly reduced motility phenotype and abnormalities of axonemal microtubules. The use of RNAi in GFP tagged cells revealed new insights to protein incorporation kinetics into the flagellum.

MATERIALS AND METHODS
Bioinformatics

Homologues were identified by reciprocal best-hit BLASTp searches using the *T. brucei* TAX-2 sequence against the predicted proteomes of *Homo sapiens* [Lander et al., 2001], *Caenorhabditis elegans*, [The *C. elegans* Sequencing Consortium, 1998], *Drosophila melanogaster* [Adams et al., 2000], *Chlamydomonas reinhardtii* (www.jgi.doe.gov), *Tetrahymena thermophila*

[Eisen et al., 2006], the Apicomplexa *Plasmodium falciparum* [Gardner et al., 2002], *Toxoplasma gondii* (www.toxodb.org) and *Cryptosporidium parvum* [Abrahamsen et al., 2004], the diatom *Thalassiosira pseudonana* [Armbrust et al., 2004] and the kinetoplastids *T. cruzi* [El-Sayed et al., 2005] and *L. major* [Ivens et al., 2005]; and the nonflagellates *Schizosaccharomyces pombe* [Wood et al., 2002], *Arabidopsis thaliana* [Arabidopsis Genome Initiative, 2000] and *Cyanidioschyzon merolae* [Matsuzaki et al., 2004]. Alignments were created using ClustalX [Thompson et al., 1997].

Constructs and Trypanosome Transfection

For TAX-2 RNAi, a 521 nucleotide fragment of the gene was amplified by PCR with TAX-2 specific primers (GTATCAGGGCACTCGGTACG, GAAGCGC GGGAATGTAATAA) incorporating XbaI and HindIII restriction sites respectively. Fragments were cloned into the p2T7-177 inducible RNAi vector [Wickstead et al., 2002] using the XbaI and HindIII sites. Procyclic form *T. brucei* 29-13 and bloodstream form *T. brucei* 90-13 cells [Wirtz et al., 1999] were transfected using standard protocols, selected using 5 μg ml^{-1} phleomycin for procyclic form cells, 2.5 μg ml^{-1} phleomycin for bloodstream form cells.

To make cell lines expressing endogenously tagged GFP:TAX-2 fusion protein, a 233 nucleotide fragment of the 5′-end of the TAX-2 gene, and a 247 nucleotide fragment within the 5′ untranslated region were amplified with specific primers incorporating suitable restriction sites and ligated into a vector for GFP expression [Kelly et al., 2007]. Procyclic form trypanosomes were transfected, and selected using 10 μg ml^{-1} blasticidin.

Culture of Trypanosomes

Procyclic cells were cultured in SDM-79 medium [Brun and Jenni, 1977] supplemented with 10% foetal calf serum and appropriate antibiotics at 28°C. Bloodstream cells were cultured in HMI-9 medium [Hirumi and Hirumi, 1989] supplemented with 15% foetal calf serum at 37°C with 5% carbon dioxide. For RNAi, cells were induced using 1 μg ml^{-1} doxycycline.

After the induction of RNAi, noninduced and induced cells were passaged to 10^6 cells per ml every 24 h by addition of cells to (preheated) SDM 79 medium containing 1 μg ml^{-1} doxycycline. Cells were counted before and after dilution using a CASY-1$^{®}$ cell counter (Schärfe, Germany). These counts were used to infer a cumulative growth curve and calculate the growth rate.

For the analysis of cells where RNAi was induced in cells expressing GFP:TAX-2, doxycycline was added to cells at 2×10^6 cells per ml, and cells were counted at each time-point where cells were fixed for GFP analysis. These counts were then used to calculate the frequency

of pre-RNAi flagella at a given time-point after induction, from the ratio of N_0/N_t.

Analysis of Motility

Noninduced cells and induced cells 72 h postinduction were grown to a density of 2×10^6 cells per ml. The motility of these cells was analysed as described by [Gadelha et al., 2005]. Images were captured every 2 s for 40 s at low magnification (10×) using phase-contrast illumination. Velocity measurements were made by tracking >50 cells over the 20 frames, using the software ImageJ (http://rsb.info.nih.gov/ij/). Chi-square and student's *t* test were carried out using Excel (Microsoft).

Fluorescence Microscopy

For imaging GFP, trypanosomes were settled onto glass slides and fixed in 2% paraformaldehyde in PBS for 10 min, after which they were permeabilised in 0.1% NP-40 in PBS and washed in PBS. Cells were embedded in Vectashield (Vector Laboratories) with 4,6-diamidino-2-phenylindole (DAPI). Slides were examined on a Zeiss Axioplan 2 microscope, captured on a CCD camera controlled by Metamorph software (Universal Imaging) and processed in Metamorph and Adobe Photoshop (Adobe). Flagella length and wveform parameters were measured in ImageJ.

Analysis of Flagellar Growth

To calculate the time taken for growth of the flagellum after cytokinesis, an analysis using the ratio of full length GFP flagella to negative distal tip flagella was carried out, similar to the analysis of Williams [1971] used by Woodward and Gull [1990]:

$$t = \tau \frac{\ln(r+1)}{\ln 2}$$

where t is the time taken for the extra growth to occur, τ is the specific growth rate and r is the ratio of ''negative distal tip'' flagella to ''full length GFP'' flagella.

Western Blotting

For immunoblotting, trypanosomes were washed twice in PBS before being resuspended in Laemmli buffer at 2.5×10^5 cells μl^{-1}. Proteins (equivalent to 2.5×10^6 cells) were transferred onto nitrocellulose membranes and stained with Ponceau-S stain before processing. The primary antibodies BB2 and Rib72 were used. Final detection was carried out using an ECL kit according to manufacturer's instructions (Perkin Elmer).

Preparation of Cells for Thin-Section TEM

Cells were fixed at 72 h after induction of RNAi in 2.5% gluteraldehyde, 2% paraformaldehyde and 0.1% picric acid in 100 mM phosphate (pH 6.5) at for 2 h at 4°C followed by postfixation in 1% osmium tetroxide in 100 mM phosphate buffer (pH 6.5) for 1 h at 4°C. The fixed material was stained en bloc with 2% aqueous uranyl acetate for 2 h at 4°C. Following dehydration through a graded series of acetone and propylene oxide, the material was embedded in epon resin for sectioning.

RESULTS

Bioinformatics Reveals TAX-2 to be Evolutionarily Conserved in Many Flagellates

The gene encoding TAX-2 (Tb10.70.7560) encodes a protein of 220 amino acids, predicted molecular weight of 25.5 kDa and predicted isoelectric point of pH 4.7. It is widely and exclusively conserved in flagellate eukaryotes, with homologues in the other kinetoplastids *Trypanosoma cruzi* and *Leishmania major*, in addition to *Homo sapiens*, *Drosophila melanogaster*, *Chlamydomonas reinhardtii*, *Giardia lamblia* and *Tetrahymena thermophila*. Notably absent from this list is the nematode *Caenorhabditis elegans* which builds only immotile sensory cilia lacking the central pair and inner and outer dynein arms; nor a is homologue found in the predicted proteome of *Thalassiosira pseudonana*, a diatom which builds a 9+0, but motile, flagellum. Searching the genomes of Apicomplexa *Plasmodium falciparum* [Gardner et al., 2002], *Toxoplasma gondii* (www.toxodb.org) and *Cryptosporidium parvum* [Abrahamsen et al., 2004] with this sequence reveals that a homologue is present only in *T. gondii*.

TAX-2 is predicted by Pfam (http://pfam.sanger.ac.uk/) to contain a Cytochrome b5-like Haem/Steroid binding domain spanning approximately the N-terminal half of the protein (Fig. 1). This domain and its position are conserved in TAX-2 homologues in other organisms, with the exception of the *D. melanogaster* protein in which no such domain was detected. BLASTp searches using the human TAX-2 homologue against the human genome reveals that there is no similarity to any other proteins outside the Cytochrome b5 domain. The structure of the Cytochrome b5 domain is known to consist of a series of β-sheets and short α-helices [Argos and Mathews, 1975], which provide a frame surrounding the central haem group. This domain is found in eukaryotes where it functions as an electron transporter [Schenkman and Jansson, 2003]. Additionally, the family of Cytochrome b5 domain-containing proteins includes progesterone binding receptors [Gerdes et al., 1998]. In this large family of proteins, the Cytochrome b5 domain is found in conjunction with many other domains, and commonly with a transmembrane helix. The transmembrane domain is not present in TAX-2, and no other domains were found.
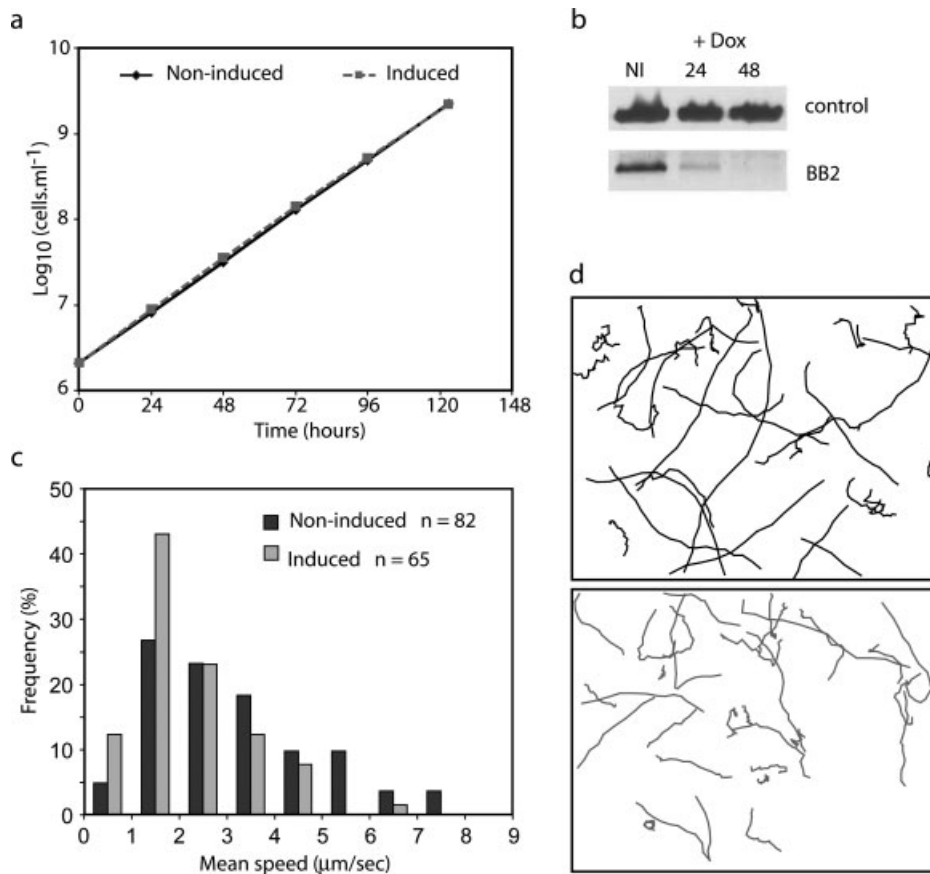
Fig. 1. TAX-2 is widely conserved in flagellates. Protein sequence alignment of *T. brucei* TAX-2 (Tb10.70.7560) with gene products from *H. sapiens*, *C. reinhardtii* (C_220104), *T. thermophila*, *T. gondii*, and *G. lamblia* with the cytochrome b5 domain spanning residues 4–120. Orthology was determined by examination of candidate sequences including reciprocal BLAST. Identical residues are shown in black boxes; similar residues are shown in light grey.

Localisation and RNAi Phenotype in Procyclic Trypanosomes

To localise TAX-2 in *T. brucei*, a strain was constructed in which one copy of the two endogenous genes in the diploid genome was replaced with a GFP:TAX-2 fusion, which contained a short Ty epitope between the GFP and TAX-2 so also allowing immunological detection with the anti-Ty epitope monoclonal antibody BB2. The GFP signal was examined in fixed cells, where it was located along the full length of the flagellum but not in the basal body, as evidenced by the gap between the kinetoplast DNA and the start of the GFP:TAX-2 signal (Figs. 3a and 3b). The signal extended from the transition zone, through the flagellar pocket and to the distal tip and was therefore clearly axonemal rather than in the paraflagellar rod (PFR). The PFR is an extra-axonemal structure present in the trypanosome flagellum only from the point of exit from the cell. To understand the function of TAX-2 in *T. brucei*, we developed a new set of vectors [Kelly et al., 2007] and applied them to use RNAi to ablate protein expression in a cell line constitutively expressing a GFP:TAX-2 fusion protein. The RNAi construct was targeted against TAX-2 mRNA and so was capable of ablating both the GFP:TAX-2 fusion and wild-type TAX-2 RNA. Expression levels of the GFP:TAX-2 could then be used for assessing the level of TAX-2 reduction. Ablation of GFP:TAX-2 could be visualised directly by the loss of GFP signal from the axoneme, and by western blotting using the anti-Ty epitope BB2 monoclonal antibody.

Ablation of TAX-2 in procyclic cells produced no effect on cell growth rate (Fig. 2a). Western blotting against the Ty epitope tag attached to GFP:TAX-2 reveals that the level of TAX-2 is much reduced by 24 h postinduction, with no band visible by 48 h postinduction (Fig. 2b). We observed that TAX-2 RNAi-induced cells continued to build a new flagellum each cell cycle. However, cell motility was slightly affected (Figs. 2c and 2d). By tracking locomotion of a cohort of individual cells in the population over the course of 40 s we were able to measure their speed. A small but statistically significant reduction in mean speed was observed between RNAi induced and noninduced cells, as shown in Fig. 2c. The average mean speed in noninduced cells was 3.2 ± 0.2 μm s^{-1}, compared with 2.2 ± 0.2 μm s^{-1} for induced cells ($P < 0.001$). Differences were also observed in the average minimum and maximum speeds between the populations of noninduced and induced cells, with induced cells having slower average minimum and maximum speeds than noninduced controls. Thus there appears to be a general reduction in motility rather than a specific loss of one component, e.g., loss of high speed motility.

In order to look for physical differences between the wave shapes that might account for the observed reduction in motility, we measured parameters of the wave including wavelength, amplitude and angle of the wave in noninduced and induced cells. We found no significant differences in any of these parameters between the two cell populations. In noninduced cells ($n = 34$),

Fig. 2.   Ablation of TAX-2 reduces motility in procyclic form trypanosomes. (**a**) Representative growth curve showing no alteration in growth kinetics in induced cells (black line) compared to noninduced controls (dashed grey line). (**b**) Western blot with BB2 antibody showing reduction in GFP:TAX-2 protein level after RNAi induction. Loading control with Rib72 shows no reduction in Rib72 protein level. (**c**) Histogram showing the frequency distribution of mean speeds of noninduced cells (black bars) and TAX-2 RNAi induced cells 72 h postinduction (grey bars). (**d**) Tracks of noninduced (black) and induced (grey) cells from which mean speeds were calculated. For each, 30 representative tracks are shown.

the mean wavelength was 5.3 ± 0.3 μm and mean amplitude was 0.9 ± 0.1 μm. In induced cells ($n = 29$), mean wavelength was 5.4 ± 0.4 μm and mean amplitude was 0.9 ± 0.1 μm. The principal angle of the bend was $87.0° \pm 4.0°$ in noninduced cells compared with $87.7° \pm 4.8°$ in induced cells.

To assess the kinetics of the loss of TAX-2, the flagella of noninduced cells and induced cells at 4, 8, 16, 24, and 48 h after induction were counted and classified by the appearance of the GFP signal. Examples of the four categories are shown in the fluorescence microscopy images in Figs. 3a–3h. GFP signal was categorised as ''full length'' (Figs. 3a and 3b), ''absent'' (Figs. 3g and 3h), ''proximal partial'' (Figs. 3e and 3f), or ''negative distal tip'' (Figs. 3c and 3d). In ''negative distal tip'' flagella the GFP signal was present from the proximal end near the basal body, along the length of the flagellum, stopping abruptly ~ 1 μm before the distal tip. In contrast, in flagella defined as ''proximal partial'' the

GFP signal decreased in intensity from proximal to distal end becoming undetectable at some point before the distal end. Figures 3i and 3j show a cell in the early stages of cell division: a new flagellum is being elongated, separating the now-replicated kinetoplasts. While the old flagellum exhibits ''full length'' GFP signal, the new flagellum exhibits GFP signal only in the proximal region, indicating the elongation of the growing new flagellum during the depletion of GFP:TAX-2.

In noninduced cells, 95% of flagella had GFP signal along the full length of the flagellum ($n = 151$). The remaining flagella were GFP negative with no detectable GFP signal in the flagellum. After induction, the frequency of ''full length GFP'' flagella decreased (Fig. 3k). Between 4 and 8 h postinduction there was a rapid increase in the number of ''proximal partial'' flagella produced which we interpret as the new flagella produced as cells became depleted of TAX-2. The frequency of ''GFP absent'' flagella increased throughout
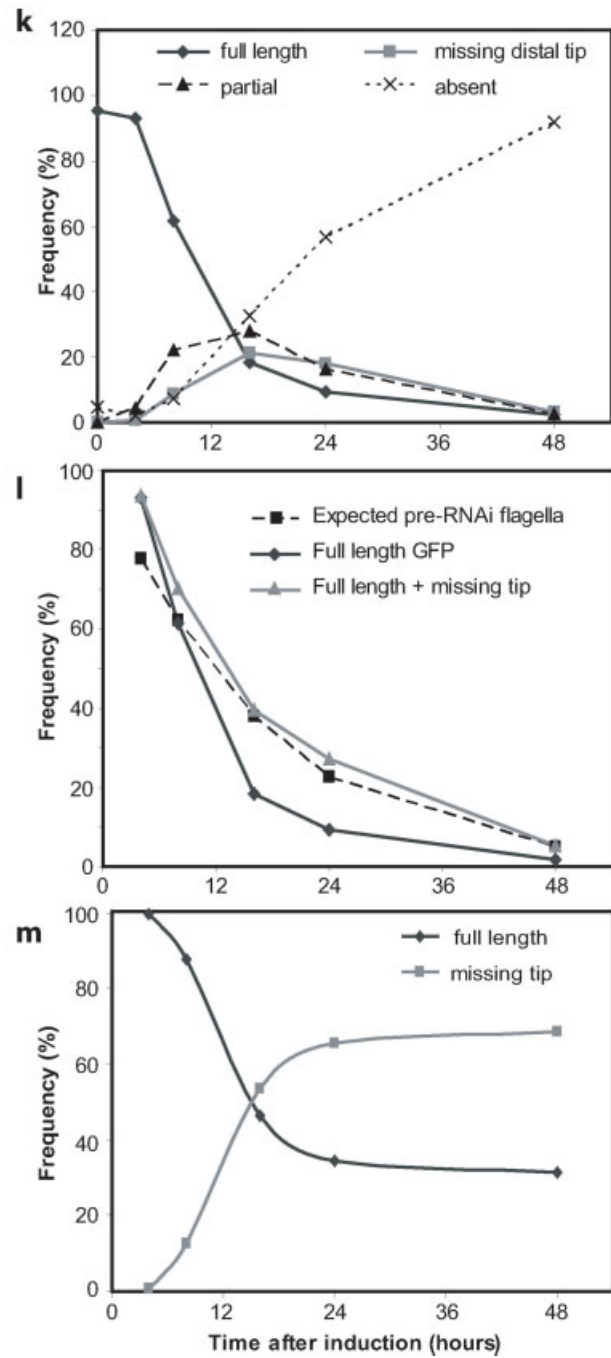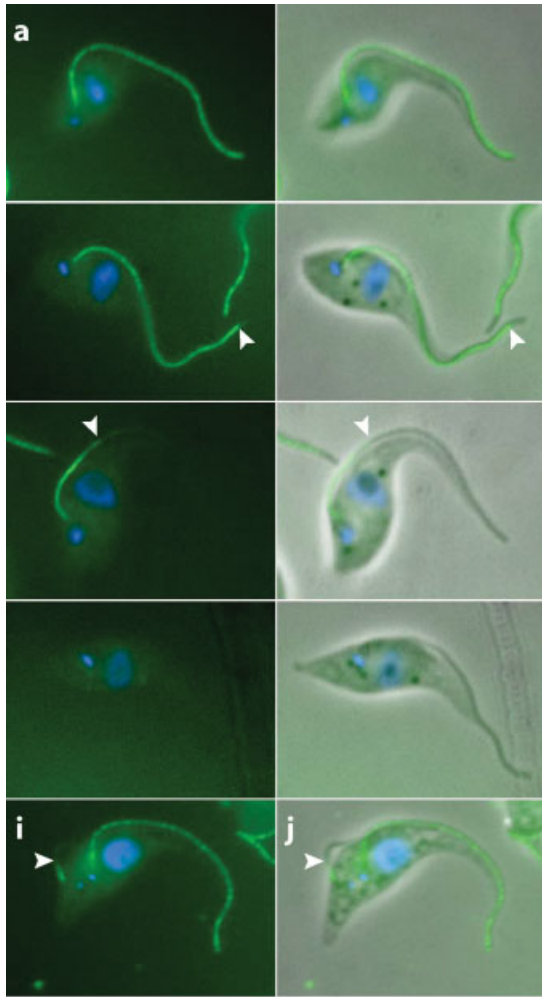
Fig. 3. Loss of GFP:TAX-2 from the axonemes of induced cells. Fluorescence (**a**, **c**, **e**, and **g**) and phase contrast microscopy (**b**, **d**, **f**, and **h**) images of induced TAX-2 RNAi cells, with DNA labeled with DAPI (blue), and native GFP (green): (a and b) cell with full length GFP flagellum; (c and d) cell with missing distal tip GFP flagellum; (e and f) cell with partial GFP flagellum; (g and h) cell with GFP negative flagellum. (**i** and **j**) cell with two flagella where the old flagellum is full length GFP and the new flagellum has GFP in the proximal part. (**k**) After induction the frequency of full length GFP flagella (solid black line) decreases; there is a temporary increase in the frequencies of partial GFP (dashed line, triangles) and missing distal tip GFP (solid grey line) flagella and a steady increase in GFP absent flagella (dashed line, crosses). (**l**) The frequency of flagella made before RNAi induction was calculated from the growth rate (dashed black line, squares); the frequency of full length GFP flagella (solid black line) is less than this, suggesting that GFP is being lost from pre-RNAi flagella; the combined frequency of full length GFP flagella and missing distal tip GFP flagella (grey line, triangles) is equal to the frequency of pre-RNAi flagella. (**m**) The ratio of full length GFP flagella to missing distal tip GFP flagella initially changes but reaches a plateau at 24 h.

the time course, reaching 92% by 48 h postinduction. Between 4 and 16 h postinduction, ''negative distal tip GFP'' flagella were produced. These could also represent new flagella produced as cells become depleted of TAX-2, but this fails to account for the clear difference in the appearance of the GFP signal between ''negative distal tip GFP'' flagella and ''proximal partial'' flagella.

As stated above, 95% of noninduced flagella are ''full length GFP''. If these flagella, made before RNAi induction (pre-RNAi flagella), retain their GFP:TAX-2 in the flagellum after RNAi induction then the frequency of ''full length GFP'' flagella should equal the frequency of pre-RNAi flagella, as calculated from the measured growth rate of the population. However, the frequency of ''full length GFP'' flagella detected drops more rapidly than can be accounted for by the assembly of axonemes after RNAi induction (Fig. 3l) suggesting that GFP:TAX-2 protein is lost from flagella after RNAi induction. However, the frequency of flagella with either ''full length GFP'' or ''negative distal tip'' closely matches that of pre-RNAi flagella. Therefore these ''negative distal tip GFP'' flagella are likely to represent flagella made before RNAi induction.

The average length of the ''negative distal tip'' region was found to be 1.1 ± 0.04 μm ($n = 44$). There are several possible explanations for this ''negative distal tip'' phenomenon: first, that there is turnover of the axoneme and this is restricted to a region at the distal tip of the flagellum; and second, that flagellar growth is not complete at cytokinesis and the new flagellum continues to grow after cytokinesis. There is a third possibility: that RNAi against TAX-2 causes the axoneme to extend in length. If this third theory is true, it should be the case that ''negative distal tip'' flagella should be longer than ''full length GFP'' flagella. We addressed this by comparing flagellar length between ''full length GFP'' flagella and ''negative distal tip GFP'' flagella. All measurements were taken from the cells which had one flagellum, or the old flagellum of cells with two flagella. We found no significant difference in the mean length of ''full length GFP'' flagella (19.8 ± 1.8 μm [$n = 105$]) compared to the mean length of ''negative distal tip GFP'' flagella (19.3 ± 1.6 μm [$n = 105$]). This suggests that the third possibility, extra growth of the flagellum caused by RNAi against TAX-2, is not the explanation for the appearance of ''negative distal tip'' flagella.

To differentiate between growth and turnover, we examined the ratio of ''full length GFP'' flagella to ''negative distal tip GFP'' flagella at 4, 8, 16, 24, and 48 h after induction (Fig. 3m). The expectation is that, if turnover is responsible, all ''full length GFP'' flagella should eventually lose the GFP signal from the tip region. Continuation of growth of new flagella made in the previous cell cycle, should however affect only these

cells, so if this explanation is correct we should observe an initial decrease in the frequency of ''full length GFP'' flagella, which should then plateau at a nonzero frequency. The plateau would occur after all those flagella made in the previous cell cycle elongate in the absence of GFP:TAX-2, while flagella that had grown to their full length before RNAi induction would remain ''full length GFP'' flagella. As shown in Fig. 3k, there is an initial change in the ratio, with a decrease in the frequency of ''full length GFP'' flagella and an increase in the frequency of ''negative distal tip GFP'' flagella, mostly occurring between 8 and 16 h postinduction. Between 24 and 48 h however there is no further change to the ratio, which remains at 1:2. This suggests that growth rather than turnover accounts for the appearance of ''negative tip GFP'' flagella. The emergence of these cells between 8 and 16 h postinduction suggests that extra growth of the flagellum after cytokinesis may continue through the early stages of at least one cell cycle, possibly more.

If we say that the ''full length GFP'' flagella at 24 h postinduction were already mature at the time of the induction and ''negative distal tip'' flagella were immature at the time of the induction (meaning that they had been built but had not completed the period of extra growth following cytokinesis), then the ratio of ''negative distal tip'' flagella to ''full length GFP'' flagella at 24 h when the plateau is reached must equal the ratio of immature to mature flagella at the time of the induction. Using this ratio it is possible to calculate how long it takes for the extra growth of the flagellum to occur, using the analysis used by Woodward and Gull [1990] to calculate the timing of events in the cell cycle. With this analysis it appears that it takes 18.5 h, or ~1.5 cell cycles, for this extra growth of the flagellum to occur, meaning that it will have already templated a new flagellum before its growth is completed.

TEM Reveals a Range of Axonemal Defects in the Flagella of RNAi-Induced Cells

RNAi-induced and noninduced cells were prepared for transmission electron microscopy and axonemal profiles examined for any defects. In noninduced cells, all axonemal profiles examined ($n = 123$) appeared as wild-type, possessing a 9+2 axoneme and PFR. Outer and inner dynein arms were visible and the central pair was positioned at the invariant position, parallel to the PFR, as is seen in wild-type *T. brucei* axonemes [Branche et al., 2006; Gadelha et al., 2006]. At 72 h postinduction, we observed that 86% of axonemes in RNAi-induced cells ($n = 98$) appeared indistinguishable from wild-type (Fig. 4). Of the remainder, a variety of axonemal defects were observed, most frequently missing outer doublets (11%). Other defects that were observed included extra
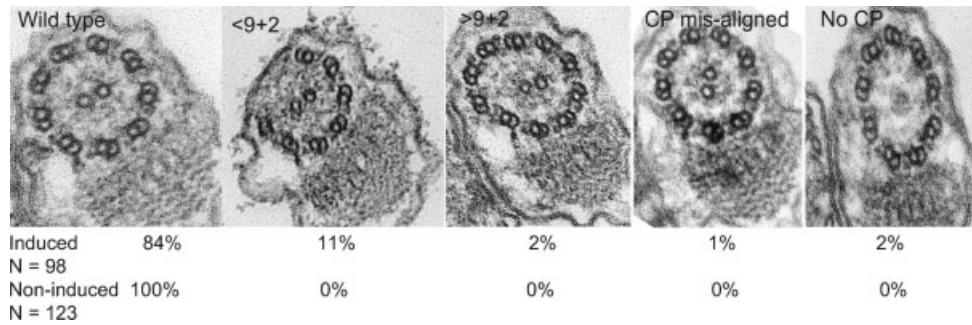
Fig. 4.   TAX-2 RNAi induction causes axonemal defects. Transmission electron microscopy images of TAX-2 noninduced (**a**) and induced (**b**–**e**) cells.

outer doublets, either incorporated into the circular profile of the axoneme or outside of it (2%); mis-alignment of the central pair (1%); or absence of the central pair (2%). The outer doublet microtubules of the trypanosome axoneme can be numbered using the PFR as an external reference, whereby doublet 1 is opposite the central pair and the furthest from the PFR. Where outer doublet microtubules were missing from an axoneme, it was most frequently the nonPFR associated doublets (8, 9, 1, 2, and 3) that were missing.

Analysis by TEM was carried out on cells which had also been examined and quantified in terms of GFP:TAX-2 signal in the flagellum. At 72 h postinduction 93% of flagella were entirely absent of GFP:TAX-2 ($n = 140$), therefore the fact that the majority of axoneme profiles are normal in appearance by TEM is not due to lack of penetrance of the RNAi. An advantage of *T. brucei* is that one can estimate the position of a cross-section along the flagellum using markers in the cell [Dawe et al., 2005]. By this means we observed that defects in axoneme structure were not restricted to the distal region but could also be found in the flagellum alongside the cell body and within the flagellar pocket, i.e., throughout the length. All basal bodies examined ($n = 23$) appeared normal in structure.

TAX-2 RNAi Induction in Bloodstream Form Cells Causes Defects in Growth and Cytokinesis

The same construct for RNAi was then used to transform bloodstream form *T. brucei* cells. Upon induction, RNAi-induced cells rapidly exhibited defects in cytokinesis and were unable to proliferate (Fig. 5a). Examination of the DAPI staining of RNAi-induced cells revealed that nuclei and kinetoplasts were able to divide and segregate, but cells did not undergo cytokinesis. A reduction in the frequency of 1K1N cells was observed, along with an increase in 2K2N cells (Fig. 5b). Successive rounds of kinetoplast segregation and mitosis produced a large number of cells with the phenotype 4K4N and 8K8N. Cells also continued to produce new flagella,

which are wrapped around the enlarged cell body in a left-handed helix (Fig. 5c). TEM revealed that many cells possessed abnormally enlarged flagellar pocket-like structures, often containing more than one flagellar profile.

Examination of the axonemes of bloodstream form cells in which RNAi had been induced revealed a variety of axonemal defects, including missing doublets (Figs. 5e and 5f), extra doublets outside of the axoneme (Fig. 5g) and rotation of the central pair (Fig. 5i), as found in the axonemes of procyclic form RNAi-induced cells. Additional defects not found in procyclic form cells were observed: flagella in which two axoneme profiles were contained within a single flagellar membrane, either complete axoneme profiles (Fig. 5i) or with doublets missing from one or both profiles (Fig. 5h). While this is not observed in procyclic form TAX-2 RNAi-induced cells, it has been observed in other flagellar RNAi cell lines in bloodstream form *T. brucei* [Broadhead et al., 2006].

DISCUSSION

TAX-2 is widely conserved with a high degree of similarity within the flagellate eukaryotes, with a high degree of similarity. Homologues were not found in all organisms that exhibit cilia / flagella however, as it appears to be absent in *Caenorhabditis elegans* and the diatom *Thalassiosira pseudonana*, which both produce axonemes lacking the central pair, radial spokes and inner dynein arms, suggesting that the function of TAX-2 may be associated with one or more of these structures. Furthermore, a TAX-2 homologue was not found in the apicomplexan *Plasmodium falciparum* which does possess an axoneme with a central pair. We know that variation in occurrence of other axonemal proteins amongst Apicomplexa (TAX-2 is present in *Toxoplasma*) likely represents genuine differences in axonemal components rather than being due to incompleteness of genomes or gene models. Several bioinformatic analyses show that
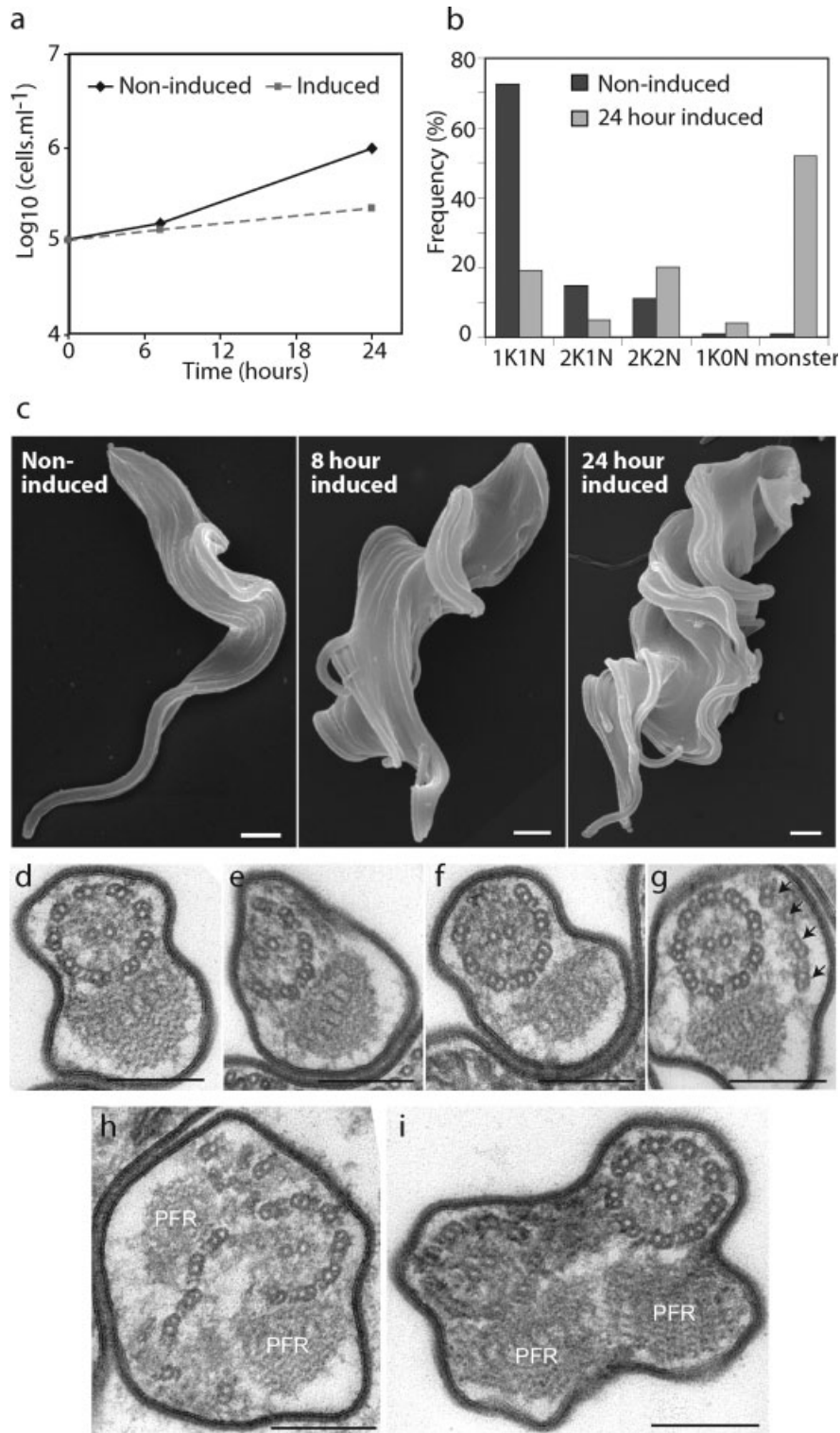
Fig. 5. TAX-2 RNAi in bloodstream form trypanosomes affects growth and cytokinesis. (**a**) Representative growth curve showing alteration in growth kinetics in induced cells (black line) compared to noninduced controls (dashed grey line). (**b**) Counts of nuclei (N) and kinetoplasts (K) in noninduced (black) and induced cells after 24 h (grey), showing a reduction in 1K1N cells and increase in cells with more than two nuclei and two kinetoplasts. (**c**) Scanning electron micrographs of a noninduced cell with one flagellum, a cell with two flagella at 8 h postinduction and a cell with at least four flagella at 24 h postinduction. Scale bars = 1 μm. (**d–i**) Transmission electron micrographs of induced cells at 24 h postinduction. (d) Axoneme with wild-type configuration. (e) Axoneme with 6+2 configuration, missing outer doublets 1, 8, and 9. (f) Axoneme with 7+2 configuration, missing outer doublets 1, 2. (g) Axoneme with 9+2 configuration and four extra outer doublets (arrows). (h) Axoneme with 7+2 configuration, missing outer doublets 7 and 8, but with extra doublets and a second paraflagellar rod (PFR) contained within the flagellar membrane. (i) Flagellar profile containing two complete axonemes and PFRs. The central pair of the axoneme on the right is misaligned. Scale bars = 200 nm.

there are distinct variations in the components of axonemes within *Plasmodium* which displays an ephemeral axoneme only in the male gamete [Briggs et al., 2004; Wickstead and Gull, unpublished observations].

TAX-2 and its homologues are predicted to contain a Cytochrome b5 heme/steroid binding domain, spanning approximately the N-terminal half of the protein. A large number of proteins contain this domain, frequently in combination with signal peptides or transmembrane domains as many are membrane-associated. To date, no other Cytochrome b5 domain-containing proteins have been identified from flagellar or ciliary proteomes. The lack of similarity to any other protein families outside of the domain region makes elucidating function by comparison difficult. It remains an intriguing domain but with no obvious candidate for a ligand.

The results of this study show that in procyclic form *T. brucei*, RNAi ablation of TAX-2 leads to a small decrease in motility. A recent general survey of flagellar components [Baron et al., 2007b] found that TAX-2 did not exhibit the phenotype of ''clumping'' which the authors attribute to defects in cytokinesis owing to reduced motility. No data are presented in that study on motility of cells, but we found no effect on growth or cytokinesis over the time period studied following RNAi against TAX-2 in procyclic form trypanosomes despite the specific reduction in motility. Structural defects were present in a minority of axonemal profiles. Similar defects have been previously observed in other RNAi cell lines: missing outer doublets are observed in the RNAi phenotype of PACRG [Dawe et al., 2005] and δ-tubulin [Gadelha et al., 2006]; absence of the central pair microtubules is produced by ablation of γ-tubulin [McKean et al., 2003]. In the PACRG and γ-tubulin mutants however, these defects lead to more extreme forms of flagellar impairment. It is possible therefore that the decrease in motility observed in the population of RNAi-induced cells comes from a minority of cells that are severely affected structurally; however this appears to be unlikely since completely paralysed cells are not observed and the majority of cells show only a slight reduction in motility. A second possibility is that these defects in axonemal structure such as are seen in Fig. 4 affect only a small region of the flagellum. TEM examination of RNAi induced cells revealed defects along the length of the flagellum, perhaps suggesting that there may be intermittent defects in axoneme structure. The defects seen in the axonemes of RNAi-induced cells by TEM suggest that TAX-2 may be involved in processes linking outer doublet microtubules to the central pair apparatus, perhaps as a part of the radial spokes or links between radial spokes and outer doublets; unfortunately, to date we have been unable to confirm this with an ultra-structural localisation for TAX-2. A function and local-

isation around the central pair would be in agreement with its longitudinal localisation to axoneme but not the basal body and transition zone where there are no central pair microtubules or radial spokes. Missing doublets could be caused as outer doublets are broken due to a loss of the connection with the central pair under the constraint of TAX-2 depletion. A break in an outer doublet could allow movement of that doublet caused by the motility of the axoneme and microtubule sliding, such that the broken doublet ''walked'' along adjacent doublets and resulting in a region with a missing doublet and further along the axoneme, a region containing an additional doublet. Of course, such a defect could also be caused by the loss of connections between the outer doublets. The presence of axonemes in which the central pair is mis-aligned or absent also suggests defects in the connections between the central pair and outer doublets. Loss of connections between the central pair and outer doublets could allow the central pair to become mis-aligned, or to break in the absence of the stability afforded by the connections to the outer doublet microtubules. Finally, the presence of a large proportion of GFP:TAX-2-negative flagella coupled with the finding that the majority of axonemes appear as wild-type by TEM demonstrates that axonemes can be built in the absence of TAX-2.

The human homologue of TAX-2, CYB5D1, is located on chromosome locus 17p13.1, a region linked to a number of retinal cone diseases. These include Leber congenital amaurosis (LCA), retinal cone dystrophy 2 (RCD2) and central areolar choroidal dystrophy (CACD). LCA is known to be caused by mutations in the retinal guanidine cyclase gene GUCY2D and arylhydrocarbon-interacting receptor protein like 1, AIPL1. Causative genes for CACD and RCD2 are not known although the region contains a number of candidate genes including GUCY2D, AIPL1, pigment epithelium-derived factor and recoverin.

The use of GFP tagging in the same cell line as RNAi ablation of both the tagged and untagged proteins provides the opportunity for studying the kinetics of protein loss directly. The novel finding that not all pre-RNAi flagella contained GFP:TAX-2 signal localising to the distal tip strongly suggested that there may be either turnover at the distal tip region or additional growth after cytokinesis. The kinetics of the change of pre-RNAi flagella from ''full length GFP'' to ''negative distal tip GFP'' indicates that the more likely explanation is additional growth of the new flagellum for some time after cytokinesis has occurred. This has been implied previously in studies where the length of the new flagellum had been compared to that of the old flagellum [Sherwin and Gull, 1989; Davidge et al., 2006; Absalon et al., 2007]. If this is a general feature of the flagellum of *T. brucei*, it should be observable in RNAi experiments

with other axonemal proteins using our new vector system to perform GFP tagging and inducible RNAi in the same cell [Kelly et al., 2007]. The results presented in this paper demonstrate that this phenomenon occurs surprisingly late—more than 1.5 cell cycles after the flagellum was first extended.

In this study we have shown a further example of a flagellar protein that dramatically affects cytokinesis and growth in the bloodstream form but not the procyclic form of *T. brucei*. Previously it has been shown that a reduction in motility in bloodstream form PFR RNAi-induced cells precedes cytokinesis defects and the accumulation of multinucleate cells [Griffiths et al., 2007]. RNAi-mediated knockdown of this protein leads to impaired motility of the flagellum in procyclic form cells however, here we show that TAX-2 knockdown in procyclic form trypanosomes causes only a slight defect in motility, with the majority of axonemes structurally unaffected. Despite this, in bloodstream forms the phenotype is as rapid and dramatic as the knockdown of flagellar proteins that have stronger procyclic motility phenotypes [Broadhead et al., 2006; Ralston and Hill, 2006]. In these cells it appears that cytokinesis fails initially as a result of loss of flagellar function [Griffiths et al., 2007]. As multiple rounds of the cell cycle occur in the absence of cytokinesis, morphogenetic axes are lost as new flagella and flagellar pockets are formed in incorrect locations [Broadhead et al., 2006]. The essential nature of motility for cytokinesis in bloodstream forms makes flagellum function a very interesting target for new therapies.

Finally, the use of an inducible RNAi system that targets both the endogenous and epitope tagged protein in the same cell provides a useful method of observing the loss and consequences of ablating a protein of interest.

ACKNOWLEDGMENTS

REFERENCES

Abrahamsen MS, Templeton TJ, Enomoto S, Abrahante JE, Zhu G, Lancto CA, Deng M, Liu C, Widmer G, Tzipori S, Buck GA, Xu P, Bankier AT, Dear PH, Konfortov BA, Spriggs HF, Iyer L, Anantharaman V, Aravind L, Kapur V. 2004. Complete genome sequence of the apicomplexan, *Cryptosporidium parvum*. Science 304:441–445.

Absalon S, Kohl L, Branche C, Blisnick T, Toutirais G, Rusconi F, Cosson J, Bonhivers M, Robinson D, Bastin P. 2007. Basal body positioning is controlled by flagellum formation in *Trypanosoma brucei*. PLoSONE 2:e437.

Adams MD, Celniker SE, Holt RA, Evans CA, Gocayne JD, Amanatides PG, Scherer SE, Li PW, Hoskins RA, Galle RF, et al. 2000. The genome sequence of *Drosophila melanogaster*. Science 287:2185–2195.

Arabidopsis Genome Initiative. 2000. Analysis of the genome sequence of the flowering plant *Arabidopsis thaliana*. Nature 408:796–815.

Argos P, Mathews FS. 1975. The structure of ferrocytochrome b5 at 2.8 A resolution. J Biol Chem 250:747–751.

Armbrust EV, Berges JA, Bowler C, Green BR, Martinez D, Putnam NH, Zhou S, Allen AE, Apt KE, Bechner M, et al. 2004. The genome of the diatom *Thalassiosira pseudonana*: ecology, evolution, and metabolism. Science 306:79–86.

Badano JL, Mitsuma N, Beales PL, Katsanis N. 2006. The ciliopathies: an emerging class of human genetic disorders. Annu Rev Genomics Hum Genet 7:125–148.

Baron DM, Kabututu ZP, Hill KL. 2007a. Stuck in reverse: loss of LC1 in *Trypanosoma brucei* disrupts outer dynein arms and leads to reverse flagellar beat and backward movement. J Cell Sci 120 (Pt 9):1513–1520.

Baron DM, Ralston KS, Kabututu ZP, Hill KL. 2007b. Functional genomics in *Trypanosoma brucei* identifies evolutionarily conserved components of motile flagella. J Cell Sci 120(Part 3): 478–491.

Bastin P, Sherwin T, Gull K. 1998. Paraflagellar rod is vital for trypanosome motility. Nature 391:548.

Branche C, Kohl L, Toutirais G, Buisson J, Cosson J, Bastin P. 2006. Conserved and specific functions of axoneme components in trypanosome motility. J Cell Sci 119(Part 16):3443–3455.

Briggs LJ, Davidge JA, Wickstead B, Ginger ML, Gull K. 2004. More than one way to build a flagellum: comparative genomics of parasitic protozoa. Curr Biol 14:R611–R612.

Broadhead R, Dawe HR, Farr H, Griffiths S, Hart SR, Portman N, Shaw MK, Ginger ML, Gaskell SJ, McKean PG, et al. 2006. Flagellar motility is required for the viability of the bloodstream trypanosome. Nature 440:224–227.

Brun R, Jenni L. 1977. A new semi-defined medium for *Trypanosoma brucei* sspp. Acta Trop 34:21–33.

Davidge JA, Chambers E, Dickinson HA, Towers K, Ginger ML, McKean PG, Gull K. 2006. Trypanosome IFT mutants provide insight into the motor location for mobility of the flagella connector and flagellar membrane formation. J Cell Sci 119(Part 19):3935–3943.

Dawe HR, Farr H, Portman N, Shaw MK, Gull K. 2005. The Parkin co-regulated gene product, PACRG, is an evolutionarily conserved axonemal protein that functions in outer-doublet microtubule morphogenesis. J Cell Sci 118(Part 23):5421–5430.

Eisen JA, Coyne RS, Wu M, Wu D, Thiagarajan M, Wortman JR, Badger JH, Ren Q, Amedeo P, Jones KM, et al. 2006. Macronuclear genome sequence of the ciliate *Tetrahymena thermophila*, a model eukaryote. PLoS Biol 4:e286.

El-Sayed NM, Myler PJ, Bartholomeu DC, Nilsson D, Aggarwal G, Tran AN, Ghedin E, Worthey EA, Delcher AL, Blandin G, et al. 2005. The genome sequence of *Trypanosoma cruzi*, etiologic agent of Chagas disease. Science 309:409–415.

Gadelha C, Wickstead B, de Souza W, Gull K, Cunha-e-Silva N. 2005. Cryptic paraflagellar rod in endosymbiont-containing kinetoplastid protozoa. Eukaryot Cell 4:516–525.

Gadelha C, Wickstead B, McKean PG, Gull K. 2006. Basal body and flagellum mutants reveal a rotational constraint of the central pair microtubules in the axonemes of trypanosomes. J Cell Sci 119(Part 12):2405–2413.

Gardner MJ, Hall N, Fung E, White O, Berriman M, Hyman RW, Carlton JM, Pain A, Nelson KE, Bowman S, et al. 2002. Genome sequence of the human malaria parasite *Plasmodium falciparum*. Nature 419:498–511.

Gerdes D, Wehling M, Leube B, Falkenstein E. 1998. Cloning and tissue expression of two putative steroid membrane receptors. Biol Chem 379:907–911.

Griffiths S, Portman N, Taylor PR, Gordon S, Ginger ML, Gull K. 2007. RNA interference mutant induction in vivo demonstrates the essential nature of trypanosome flagellar function during mammalian infection. Eukaryot Cell 6:1248–1250.

Hirumi H, Hirumi K. 1989. Continuous cultivation of *Trypanosoma brucei* blood stream forms in a medium containing a low concentration of serum protein without feeder cell layers. J Parasitol 75:985–989.

Hutchings NR, Donelson JE, Hill KL. 2002. Trypanin is a cytoskeletal linker protein and is required for cell motility in African trypanosomes. J Cell Biol 156:867–877.

Ivens AC, Peacock CS, Worthey EA, Murphy L, Aggarwal G, Berriman M, Sisk E, Rajandream MA, Adlem E, Aert R, et al. 2005. The genome of the kinetoplastid parasite, Leishmania major. Science 309:436–442.

Kelly S, Reed J, Kramer S, Ellis L, Webb H, Sunter J, Salje J, Marinsek N, Gull K, Wickstead B, et al. 2007. Functional genomics in *Trypanosoma brucei*: a collection of vectors for the expression of tagged proteins from endogenous and ectopic gene loci. Mol Biochem Parasitol 154:103–109.

Lander ES, Linton LM, Birren B, Nusbaum C, Zody MC, Baldwin J, Devon K, Dewar K, Doyle M, FitzHugh W, et al. 2001. Initial sequencing and analysis of the human genome. Nature 409:860–921.

Matsuzaki M, Misumi O, Shin IT, Maruyama S, Takahara M, Miyagishima SY, Mori T, Nishida K, Yagisawa F, Nishida K, et al. 2004. Genome sequence of the ultrasmall unicellular red alga *Cyanidioschyzon merolae* 10D. Nature 428:653–657.

McKean PG, Baines A, Vaughan S, Gull K. 2003. Gamma-tubulin functions in the nucleation of a discrete subset of microtubules in the eukaryotic flagellum. Curr Biol 13:598–602.

Pazour GJ, Agrin N, Leszyk J, Witman GB. 2005. Proteomic analysis of a eukaryotic cilium. J Cell Biol 170:103–113.

Ralston KS, Hill KL. 2006. Trypanin, a component of the flagellar dynein regulatory complex, is essential in bloodstream form African trypanosomes. PLoS Pathog 2:e101.

Schenkman JB, Jansson I. 2003. The many roles of cytochrome b5. Pharmacol Ther 97:139–152.

Sherwin T, Gull K. 1989. The cell division cycle of *Trypanosoma brucei brucei*: timing of event markers and cytoskeletal modulations. Philos Trans R Soc Lond B Biol Sci 323:573–588.

Stolc V, Samanta MP, Tongprasit W, Marshall WF. 2005. Genome-wide transcriptional analysis of flagellar regeneration in *Chlamydomonas reinhardtii* identifies orthologs of ciliary disease genes. Proc Natl Acad Sci USA 102:3703–3707.

The *C. elegans* Sequencing Consortium. 1998. Genome sequence of the nematode *C. elegans*: a platform for investigating biology. Science 282:2012–2018.

Thompson JD, Gibson TJ, Plewniak F, Jeanmougin F, Higgins DG. 1997. The CLUSTAL_X windows interface: flexible strategies for multiple sequence alignment aided by quality analysis tools. Nucleic Acids Res 25:4876–4882.

Wickstead B, Ersfeld K, Gull K. 2002. Targeting of a tetracycline-inducible expression system to the transcriptionally silent minichromosomes of *Trypanosoma brucei*. Mol Biochem Parasitol 125:211–216.

Williams FM. 1971. Dynamics of microbial populations. In: Patten B, editor. Systems Analysis and Simulation Ecology. New York: Academic press. pp 247–262.

Wirtz E, Leal S, Ochatt C, Cross GA. 1999. A tightly regulated inducible expression system for conditional gene knock-outs and dominant-negative genetics in *Trypanosoma brucei*. Mol Biochem Parasitol 99:89–101.

Wood V, Gwilliam R, Rajandream MA, Lyne M, Lyne R, Stewart A, Sgouros J, Peat N, Hayles J, Baker S, et al. 2002. The genome sequence of *Schizosaccharomyces pombe*. Nature 415:871–880.

Woodward R, Gull K. 1990. Timing of nuclear and kinetoplast DNA replication and early morphological events in the cell cycle of *Trypanosoma brucei*. J Cell Sci 95(Part 1):49–57.